

State-space PTA

Kimpson¹, Melatos, O’Leary, Evans, others, etc. etc. ^{★†}

¹*Royal Astronomical Society, Burlington House, Piccadilly, London W1J 0BQ, UK*

Last updated 2020 June 10; in original form 2013 September 5

ABSTRACT

This is an abstract

Key words: editorials, notices – miscellaneous

1 INTRODUCTION

The detection of high frequency (~ 1 Hz) gravitational waves (GWs) from coalescing black hole (BH) binaries with ground-based detectors such as LIGO/Virgo (LIGO Scientific Collaboration et al. 2015; Acernese et al. 2015) is now a routine enterprise (e.g. Abbott et al. 2019, 2021). Gravitational radiation from sources which radiate in the mill-Hz regime are expected to be detectable from ~ 2037 with the space-based Laser Interferometer Space Antenna, (Amaro-Seoane et al. 2017), especially given the early success by the pathfinder mission (Armano et al. 2019). Detecting GWs from systems which evolve over even longer timescales, $O(\text{years})$, has necessitated the development of novel astrophysical methods, since it is practically impossible to engineer interferometric detectors with sufficiently long baselines. The foremost technique for the detection of GWs in this nano-Hz regime is a via timing an ensemble of milliseconds pulsars; a pulsar timing array (PTA) (Verbiest et al. 2021). The presence of a nano-Hz gravitational wave will influence the propagation of the pulsar radio beacon, leaving a characteristic impression on the pulsar timing signal. By measuring the modulation of the received pulsar signal in this way, one can effectively construct a detector with a baseline on the scale of parsecs.

Multiple PTA detectors have now been built over the last few decades, including the North American Nanohertz Observatory for Gravitational Waves (NANOGrav, Arzoumanian et al. 2020), the Parkes Pulsar Timing array (PPTA Kerr et al. 2020), and the European Pulsar Timing Array (EPTA, Ferdman et al. 2010). These previously disparate efforts have now been joined in international collaboration, along with a number of newer PTAs such as the Indian Pulsar Timing Array Project (InPTA, Tarafdar et al. 2022), under the umbrella of the International Pulsar Timing Array (IPTA Perera et al. 2019). The primary target of PTA observations is the gravitational radiation emitted from the inspiral of supermassive black hole binaries (SMBHBs) with masses $\sim 10^7 M_\odot$. These GW signals from SMBHBs can be broadly classified into either deterministic or stochastic. For the former, sufficiently bright and near binaries may be resolvable with PTAs, allowing the very earliest stages of their evolution and coalescence to be investigated (Zhu et al. 2015). For

the latter, the incoherent superposition of multiple weaker SMBHBs sources leads to a stochastic background detectable at nano-Hz frequencies (Sesana et al. 2008). Other potential sources for PTAs include cosmic strings (e.g. Sanidas et al. 2012) and cosmological phase transitions (e.g. Xue et al. 2021), but the deterministic and stochastic GW signals from SMBHBs remain the primary targets.

The detection of loud, resolved sources with a PTA typically involves a parametrised model for the pulsar timing residuals induced by the modulation of the pulsar signal by a GW. One can then search for evidence that this model describes the data via the usual Bayesian likelihood techniques, and try to estimate the parameters of the model (e.g. Babak et al. 2016). For detecting the stochastic background the approach is different; one measures the correlation in pulsar timing residuals between any two pair of pulsars. The presence of a GW induces a characteristic correlation function as a function of the angular separation between the pulsars; the Hellings-Downs curve (Hellings & Downs 1983). For both classes of source, the detection of GW signals in the timing residuals of a PTA is a challenging enterprise, and currently neither a stochastic background nor an individually resolved source has yet been detected (Antoniadis et al. 2022; Hobbs & Dai 2017).

The sensitivity of a PTA to a GW signal is heavily dependent on the total level of noise in the array (Wang 2015). In particular, the intrinsic pulsar timing noise - i.e. random variations in the pulse arrival time - has been identified as a key factor limiting the sensitivity of PTAs to GW signals (Shannon & Cordes 2010; Lasky et al. 2015; Caballero et al. 2016). This pulsar timing noise has multiple potential theorized causes including microglitches (Melatos et al. 2008), glitch recovery (Hobbs et al. 2010), fluctuations in both the internal and external stochastic torques (Antonelli et al. 2023) and superfluid turbulence (Melatos & Link 2014). In order to mitigate the influence of timing noise, PTAs are typically composed of millisecond pulsars (MSPs) which are known to be much more stable rotators with minimal timing noise. However, timing noise in MSPs could be a ‘latent’ phenomenon (Shannon & Cordes 2010); as we increase the length of observation spans and the measurement timing precision to the levels required to detect gravitational waves, the timing noise in MSPs may emerge and become much more apparent, visible in the same way that timing noise is seen in younger pulsars. In addition to timing noise there are also secondary noise sources that must be considered such as phase jitter noise and radiometer noise

[★] Contact e-mail: mn@ras.ac.uk

[†] Present address: Science magazine, AAAS Science International, 82-88 Hills Road, Cambridge CB2 1LQ, UK

(Cordes & Shannon 2010; Lam et al. 2019; Parthasarathy et al. 2021).

In the standard approach to PTA-GW analysis, timing noise is a nuisance which must be accurately modelled and subtracted. It fundamentally limits the sensitivity of the PTA detector to a GW signal, and the ability of an observer to infer the GW source parameters. Motivated by these challenges faced by the classic PTA analysis methods, in this work we present a novel approach to formulate PTA analysis and GW detection as a state-space problem. This approach enables the pulsar state-space evolution to be tracked optimally, given a specific realisation of the pulsar process noise (i.e. the spin wandering of the pulsar), and determine both the presence of a GW signal in the pulsar data, and infer the underlying source parameters. For this initial exploratory study we will focus exclusively on resolved, monochromatic GW sources. **TK: This motivation section is weak. Need to think about how to phrase this better. Be clear on the real challenges of the "old" approach and the advantages of the "new" one.**

This is how we usually search for single source PTAs
estimate all unknown parameters optimally here is a difference approach

Typical approaches for

This paper is organised as follows: **TK: TBD**

We adopt the natural units, with $c = G = \hbar = 1$, and a $(-, +, +, +)$ metric signature.

2 STATE-SPACE MODEL

We want to formulate the PTA analysis as a state-space problem with a separation between the intrinsic pulsar state, and the measurement state recorded by an observer. For this work we will take our state variable to be the intrinsic pulsar pulse frequency $f_p(t)$, as measured in the momentarily comoving reference frame of an observer local to the pulsar. We will take our measurement variable to be the pulsar pulse frequency that is measured by an observer at Earth, $f_m(t)$. In Sections 2.1, 2.2 we will describe our model for $f_p(t)$ and $f_m(t)$ respectively. We will go on in Section 3.1 to bring together these two models into a cohesive, discretized state space model. **TK: Need some extra discussion here on why this choice of state/measurement space. Why not e.g. phase, TOA, voltage, etc. ?**

2.1 Evolution of the pulsar frequency

We will take as our model of the intrinsic pulsar frequency $f_p(t)$ a variation of the phenomenological model of Vargas & Melatos (2023). Within this model, $f_p(t)$ evolves according to a combination of both deterministic torques (i.e. electromagnetic spin-down) and stochastic torques (i.e. ‘spin wandering’, achromatic variations in the pulse TOA intrinsic to the star). The deterministic torque is taken to arise from the pulsar magnetic dipole, with braking index $n = 3$ whilst the stochastic torque is a simple white noise process. Specifically, the frequency evolves according to a Ornstein-Uhlenbeck process (equivalently a Langevin equation) with a time-dependent drift parameter:

$$\frac{df_p}{dt} = -\gamma[f_p - f_{EM}(t)] + \dot{f}_{EM} + \xi(t) \quad (1)$$

where f_{EM} is the solution of the electromagnetic spindown equation, \dot{f}_{EM} is the spin derivative, γ a proportionality constant that specifies

the mean-reversion timescale, and $\xi(t)$ a white noise process that satisfies,

$$\langle \xi(t)\xi(t') \rangle = \sigma^2 \delta(t - t') \quad (2)$$

for variance σ^2 . For PTA analysis, we are concerned with timescales on the order of years. Consequently, we can express the EM spindown straightforwardly as

$$\dot{f}_{EM}(t) = f_{EM}(0) + \dot{f}_{EM}(0)t \quad (3)$$

Completely, the frequency evolution is then given by the solution of the stochastic differential equation,

$$\frac{df_p}{dt} = -\gamma[f_p - f_{EM}(0) - \dot{f}_{EM}(0)t] + \dot{f}_{EM}(0) + \xi(t) \quad (4)$$

As emphasised in Vargas & Melatos (2023), this model for the frequency evolution is a phenomenological model that aims to qualitatively reproduce the typical behaviour of observed pulsars, rather than being derived from a physical model of the neutron star (e.g. a model of the neutron star crust and superfluid, components Meyers et al. 2021). For our purposes of exploring the detection of GWs via a state space formulation it will prove sufficiently accurate and appropriate.

2.2 Modulation of pulsar frequency due to a GW

In the presence of a GW, the pulse frequency measured by an observer in the local neutron star reference frame is different from that measured by an observer on Earth. We will now derive the influence of the GW on the received pulse frequency.

2.2.1 Plane GW perturbation

We take a gravitational plane wave that perturbs a background Minkowski spacetime as

$$g_{\mu\nu} = \eta_{\mu\nu} + H_{\mu\nu} e^{i(\Omega(\bar{n} \cdot \bar{x} - t) + \Phi_0)} \quad (5)$$

for Minkowski metric $\eta_{\mu\nu}$, spatial coordinates \bar{x} , where the GW has a constant angular frequency Ω , propagates in the \bar{n} -direction and has a phase offset of Φ_0 . We emphasise that for this work Ω has no time dependence - we are concerned solely with monochromatic sources. We are free to choose our coordinate system such that Φ_0 is the GW phase at $t = 0$ at the Earth. The amplitude tensor $H_{\mu\nu}$ has zero temporal components ($H_{0\mu} = H_{\mu 0} = 0$) whilst the spatial part is

$$H_{ij} = h_+ e_{ij}^+(\bar{n}) + h_\times e_{ij}^\times(\bar{n}) \quad (6)$$

where h_+, \times are the polarisation amplitudes of the gravitational plane wave which are given by

$$h_+ = h(1 + \cos^2 \iota) \quad (7)$$

$$h_\times = -2h \cos \iota \quad (8)$$

The polarisation tensors $e_{ij}^{+,\times}$ are uniquely defined by the principal axes of the wave:

$$e_{ab}^+(\hat{\Omega}) = \hat{m}_a \hat{m}_b - \hat{n}_a \hat{n}_b \quad (9)$$

$$e_{ab}^\times(\hat{\Omega}) = \hat{m}_a \hat{n}_b + \hat{n}_a \hat{m}_b \quad (10)$$

which are in turn specified via the location of the GW source on the sky (via polar coordinate θ and azimuthal coordinate ϕ) and the

polarisation angle ψ

$$\begin{aligned}\vec{m} = & (\sin \phi \cos \psi - \sin \psi \cos \phi \cos \theta) \hat{x} \\ & - (\cos \phi \cos \psi + \sin \psi \sin \phi \cos \theta) \hat{y} \\ & + (\sin \psi \sin \theta) \hat{z}\end{aligned}\quad (11)$$

$$\begin{aligned}\vec{n} = & (-\sin \phi \sin \psi - \cos \psi \cos \phi \cos \theta) \hat{x} \\ & + (\cos \phi \sin \psi - \cos \psi \sin \phi \cos \theta) \hat{y} \\ & + (\cos \psi \sin \theta) \hat{z}\end{aligned}\quad (12)$$

2.2.2 Pulse frequency as a photon

We will consider the pulse frequency as a photon with covariant 4-momentum p_μ . Generally, the frequency of a photon recorded by an observer with 4-velocity u^μ is

$$f = p_\alpha u^\alpha \quad (13)$$

We consider both our emitter and receiver to be stationary, such that

$$u^\alpha|_{\text{emitter}} = u^\alpha|_{\text{receiver}} = (1, 0, 0, 0) \quad (14)$$

Consequently the frequency can be directly identified with the temporal component of the covariant 4-momentum,

$$f = p_t \quad (15)$$

The expression for the evolution of the pulse frequency as measured by the observer on Earth is then,

$$p_t(t_1)|_{\text{Earth}} = p_t(t_0)|_{\text{source}} + \int_{t=t_0}^{t=t_1} \dot{p}_t dt \quad (16)$$

where the overdot denotes a derivative w.r.t. t . Since the influence of the GW perturbation on \dot{p}_t is small, we can relate the source emission and receiver times as $t_1 = t_0 + d$ and consider the photon trajectory to be an unperturbed path.

2.2.3 Hamiltonian Mechanics

The Hamiltonian in covariant notation can be written as

$$H = \frac{1}{2} g_{\mu\nu} p^\mu p^\nu, \quad (17)$$

which if we substitute in our expression for the perturbed metric is

$$H = \frac{1}{2} \eta_{\mu\nu} p^\mu p^\nu + \frac{1}{2} H_{ij} p^i p^j e^{i(\Omega(\vec{n} \cdot \vec{x} - t) + \Phi_0)} \quad (18)$$

Now, Hamilton's equations are

$$\frac{dx^\mu}{d\lambda} = \frac{\partial H}{\partial p_\mu}, \quad \frac{dp_\mu}{d\lambda} = -\frac{\partial H}{\partial x^\mu} \quad (19)$$

for affine parameter λ . The derivative of the temporal component of the covariant momenta is then,

$$\frac{dp_t}{d\lambda} = -\frac{i\Omega}{2} H_{ij} p^i p^j e^{i(\Omega(\vec{n} \cdot \vec{x} - t) + \Phi_0)} \quad (20)$$

The derivative w.r.t coordinate time t is

$$\dot{p}_t = \frac{dp_t}{d\lambda} \left(\frac{d\lambda}{dt} \right)^{-1} = \frac{dp_t}{d\lambda} \left(\frac{1}{p^t} \right) \quad (21)$$

Note that \dot{p}_t is entirely a function of the GW perturbation. In the Minkowski case the spacetime is stationary and so p_t should be conserved along the geodesic. It will prove useful to recognise that

$$p^\mu = \omega(1, -q^x, -q^y, -q^z) \quad (22)$$

where \vec{q} is the unit vector between the Earth and pulsar and ω is the

constant photon angular frequency. Given the small effect of the GW perturbation, at first order we can identify ω as either the frequency at source or observer. Similarly, we can parameterize the photon spatial coordinates \vec{x} as,

$$\vec{x}(t) = -\vec{q}(t - t_1) \quad (23)$$

Note that when our integration variable $t = t_1$ (i.e. the photon is at Earth) then $\vec{x}(t = t_1) = 0$ which is what we expect given our chosen coordinate system. Also note that \dot{p}_t is entirely a function of the GW perturbation. In the Minkowski case the spacetime is stationary and so p_t should be conserved along the geodesic. We will treat the pulsar locations to be constant with respect to the Earth, i.e. \vec{q} is not a function of time. In practice, the pulsar locations vary with respect to the Earth, but are constant with respect to the solar system barycentre (SSB). This barycentering correction is typically applied during the pulsar detection process. Our conclusions are generally unchanged by this choice - it is straightforward to transform q if needed into a vector between the SSB and pulsar.

Bringing this all together we can write \dot{p}_t in a condensed form as,

$$\dot{p}_t = A e^{iBt+C} \quad (24)$$

with

$$A = -\frac{i\Omega\omega}{2} H_{ij} q^i q^j \quad (25)$$

$$B = -\Omega(1 + \vec{n} \cdot \vec{q}) \quad (26)$$

and

$$C = \Omega\tau\vec{n} \cdot \vec{q} + \Phi_0 \quad (27)$$

From Eq 16 the frequency shift experienced by the observer relative to the source due to a GW is then

$$p_t(\tau)|_{\text{Earth}} - p_t(\tau - d)|_{\text{source}} = \quad (28)$$

$$A \int_{t=\tau-d}^{t=\tau} e^{iBt+C} dt \quad (29)$$

$$= \frac{-iA}{B} e^{i(-\Omega\tau+\Phi_0)} \left(1 - e^{-iBd} \right) \quad (30)$$

$$= \frac{\omega}{2} \frac{h_{ij}(\tau; \vec{x} = 0) q^i q^j}{(1 + \vec{n} \cdot \vec{q})} \left(1 - e^{i\Omega(1+\vec{n} \cdot \vec{q})d} \right) \quad (31)$$

for $h_{ij} = g_{ij} - \eta_{ij}$. Since via Equation 13 we can related the temporal component of the covariant momentum to the frequency, it follows that

$$f(\tau)|_{\text{Earth}} = f(\tau - d)|_{\text{source}} \left(1 - \frac{\omega}{2} \frac{h_{ij}(\tau; \vec{x} = 0) q^i q^j}{(1 + \vec{n} \cdot \vec{q})} \left(1 - e^{i\Omega(1+\vec{n} \cdot \vec{q})d} \right) \right) \quad (32)$$

where we have identified ω with $f(\tau - d)|_{\text{source}}$.

3 DETECTION AND PARAMETER ESTIMATION

Let's review and categorise all the free parameters, $\vec{\theta}$, of above model. We can generally separate these into parameters which correspond to the intrinsic frequency evolution of the pulsar and parameters of the GW source

$$\vec{\theta} = \vec{\theta}_{\text{PSR}} \cup \vec{\theta}_{\text{GW}} \quad (33)$$

$$\vec{\theta}_{\text{PSR}} = [\gamma, f_{\text{EM}}(0), \dot{f}_{\text{EM}}(0), d]^{(N)} \quad (34)$$

$$\bar{\theta}_{\text{GW}} = [h_+, h_\times, \delta, \alpha, \psi, \Omega, \Phi_0] \quad (35)$$

Whilst the GW parameters are shared between measurements for each pulsar, the pulsar parameters are clearly not. For a PTA dataset of N pulsars we have $7 + 5N$ parameters to estimate. Note that whilst this is a large parameter space, in general the pulsar parameters are much better constrained than the GW parameters: for example we have rough estimates for the pulsar distances accurate to $\sim 10\%$, but we have no prior information on the source location.

In this section we present a new method to infer the model parameters and calculate the marginal likelihood (i.e. the model evidence). In Section 3.1 we will present a discretised version of the model of Section 2 which maps onto the discretely sampled observable $f(\tau)|_{\text{Earth}}$. In Section 3.2 we will outline how observations of this pulse frequency can be used to recover the underlying intrinsic pulsar state $f(\tau - d)|_{\text{source}}$ using a Kalman Filter. In Section 3.3 we will demonstrate how to deploy the Kalman filter in conjunction with a nested sampling technique to recover the model parameters. We will now review the Kalman filter and the associated likelihood in Section 3.2 before going on in Section 3.3 to discuss how to use nested sampling methods together with the filter for detection (model selection) and parameter estimation.

3.1 Discretised model

We can express the intrinsic frequency evolution, Eq. 4, in an alternative form as,

$$df = \mathcal{A}f dt + N(t)dt + \sigma dB(t) \quad (36)$$

where $\mathcal{A} = -\gamma$, $N(t) = \gamma(f_{\text{EM}}(0) + \dot{f}_{\text{EM}}(0)t + \ddot{f}_{\text{EM}}(0))$ and $dB(t)$ denotes increments of Brownian motion (Wiener process). This equation is easily identified as an Ornstein-Uhlenbeck process which has a general solution given by (Gardiner 2009),

$$f(t) = e^{\mathcal{A}t} f(0) + \int_0^t e^{\mathcal{A}(t-t')} N(t') dt' + \int_0^t e^{\mathcal{A}(t-t')} \sigma dB(t') \quad (37)$$

If we move from a solution in continuous time, t , to discrete time, $\bar{t} = (t_1, t_2, \dots, t_K)$, then

$$f(t_{i+1}) = F f(t_i) + T_i + \eta_i \quad (38)$$

where

$$F_i = e^{\mathcal{A}(t_{i+1}-t_i)} \quad (39)$$

$$T_i = \int_{t_i}^{t_{i+1}} e^{\mathcal{A}(t_{i+1}-t')} N(t') dt' \quad (40)$$

$$\eta_i = \int_{t_i}^{t_{i+1}} e^{\mathcal{A}(t_{i+1}-t')} \sigma dt' \quad (41)$$

The discrete solution $f(\bar{t})$ to the intrinsic frequency can be related to the discrete measured frequency via Eq. 32 as,

$$f_M(\bar{t}) = f(\bar{t})g(\bar{\theta}, \bar{t}) + N_M \quad (42)$$

where $g(\theta, t)$ can be expressed in a trigonometric form as

$$X = 1 - \frac{1}{2} \frac{H_{ij} q^i q^j}{(1 + \bar{n} \cdot \bar{q})} [\cos(-\Omega\tau + \Phi_0) - \cos(-\Omega\tau + \Phi_0 + \Omega(1 + \bar{n} \cdot \bar{q})d)]$$

whilst N_M is a Gaussian measurement noise that satisfies

$$\langle N_M(t) N_M(t') \rangle = \Sigma^2 \delta(t - t') \quad (44)$$

for variance Σ^2 .

3.2 Kalman Filtering

The Kalman filter (Kalman 1960) is a algorithmic technique for recovering a set of system state variables, \bar{x} , given some noisy measurements, \bar{z} . It is a common technique in signal processing that has also been applied more recently with great success in astrophysics (e.g. Meyers et al. 2021; Melatos et al. 2021). The linear Kalman filter operates on measurements that are related to states via a linear transformation

$$\bar{z} = \bar{H}\bar{x} + \bar{v} \quad (45)$$

where \bar{H} is the measurement matrix and \bar{v} a Gaussian measurement noise. The underlying states are the solutions to the state-space equation

$$\dot{\bar{x}} = \bar{F}\bar{x} + \bar{G}\bar{u} + \bar{w} \quad (46)$$

for the system dynamics matrix, \bar{F} , control model \bar{G} , control vector \bar{u} , and w a stochastic zero-mean process. By comparison with the preceding equations, Eqs. 36 - ??, it is immediately obvious how our state space model maps onto the Kalman filter structure. Specifically, our states are just the N intrinsic pulsar frequencies $\bar{x} = (f_1, f_2, \dots, f_N)$ whilst our measurements are the N measured pulse frequencies $\bar{z} = (f_1^{(M)}, f_2^{(M)}, \dots, f_N^{(M)})$. If we specialize to the case of constant time sampling between our observations, Δt , then for our formulation the components that make up the Kalman filter are as follows:

$$F_i = F_{i+1} = e^{-\gamma\Delta t} \quad (47)$$

$$T_i = \int_{t_i}^{t_{i+1}} e^{A(t_{i+1}-t')} N(t') dt' \quad (48)$$

$$= f_{\text{EM}}(0) + \dot{f}_{\text{EM}}(0)(\Delta t + t_i) - e^{-\gamma\Delta t} (f_{\text{EM}}(0) + \dot{f}_{\text{EM}}(0)t_i) \quad (49)$$

$$H_i = 1 - A(\theta_{\text{GW}}) \cos(-\Omega t_i(1 + \bar{n} \cdot \bar{q}) + \Phi_0) \quad (50)$$

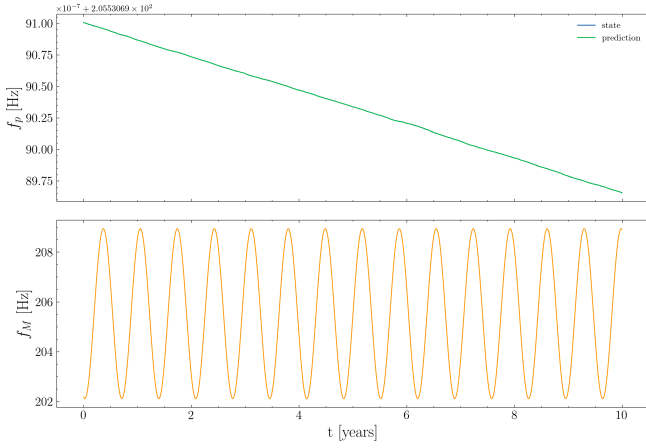
where the i subscript labels the value at the i -th timestep, and A is a constant that is given by Eq. ??.

The Kalman filter includes the effect of process noise \bar{w} and the measurement noise \bar{v} via the definition of a process noise matrix $Q = E[\bar{w}\bar{w}^T]$ and a measurement noise matrix $R = E[\bar{v}\bar{v}^T]$, which have the discrete form,

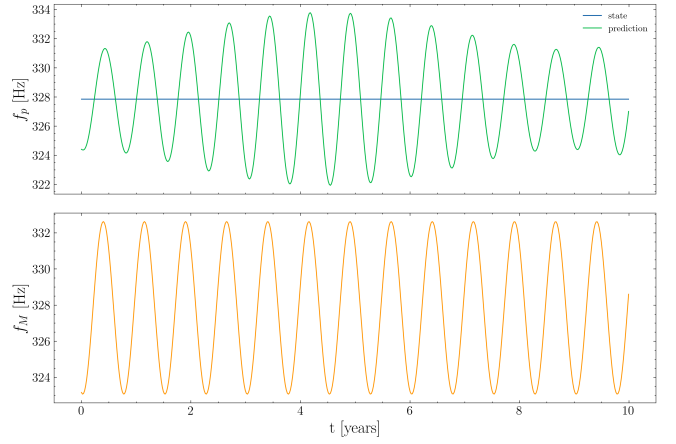
$$Q_i \delta_{ij} = \langle \eta_i \eta_j^T \rangle = \frac{-\sigma^2}{2\gamma} (e^{-2\gamma\Delta t} - 1) \quad (51)$$

$$R_i = R_{i+1} = \Sigma^2 \quad (52)$$

The above equations, Eqs. 47 - 52, apply to an operation on a single state. The extension to N states is straightforward, since one just needs to construct a diagonal matrix for each of the Kalman components where each non-zero element corresponds to a separate pulsar frequency. For our formulation we are concerned only with the linear Kalman filter since the measurements are a linear function of the states and the state transitions are also linear. Extension to



(a) Using correct parameters



(b) Using incorrect parameters

Figure 1. Application of a Kalman filter to recover the intrinsic frequency states (top panels) given a measured frequency signal (bottom panels) which has been modulated by the presence of a gravitational wave. In the case where the parameters of the filter are accurate (subfigure (a)) the underlying states are also recovered accurately. Conversely, when the parameters fed to the filter are inaccurate (subfigure (b)) the filter cannot recover the state. **TK: this needs to be just one stacked figure.**

non-linear problems is straightforward using either an extended Kalman filter (Zarchan & Musoff 2000), the unscented Kalman filter (Wan & Van Der Merwe 2000) or the particle filter (Simon 2006). For a full review of the Kalman filter equations in an astrophysical context, which may be unfamiliar to some, we refer the reader to the appendices of Melatos et al. (2021) and Meyers et al. (2021).

In order for the Kalman filter to function successfully, the parameters of the model, which appear in the various Kalman matrices, must be accurate. Erroneous or inaccurate parameters lead to inaccurate predictions of the underlying states (e.g. Fig 1). The filter tracks the error in its predictions of the underlying states by projecting the state predictions back into measurement space, $\hat{x} \rightarrow \hat{z}$. These measurement predictions can then be compared against the true observed measurements i.e. $\epsilon = \bar{z} - \hat{z}$. The Gaussian log-likelihood at timestep i , as a function of the parameters is,

$$\log \mathcal{L}_i = -\frac{1}{2} (N \log 2\pi + \log \det |S_i| + \epsilon_i^T S_i^{-1} \epsilon_i) \quad (53)$$

where S_i is the covariance matrix of the error ϵ_i . The net log-likelihood is simply the sum over all timesteps.

3.3 Nested Sampling

Nested Sampling (Skilling 2006) is an integration algorithm used for evaluating integrals of the Bayesian evidence form,

$$Z = \int \mathcal{L}\pi(\theta) d\theta \quad (54)$$

where $\pi(\theta)$ is the prior which is a function of a set of unknown parameters θ . The primary advantage of nested sampling is the ability to compute this evidence integral, which is key for model selection, and proves difficult without considerable extra cost for the usual Markov Chain Monte Carlo (MCMC) approaches. Nested sampling is also typically less computationally intensive than MCMC and can handle multi-modal problems (Ashton et al. 2022). For these reasons, it has enjoyed widespread adoption in the physical sciences, particularly within the cosmological community (Mukherjee et al. 2006; Feroz & Hobson 2008; Handley et al. 2015), but has also commonly been applied in astrophysics (Buchner 2021),

particle physics (Trassinelli 2019) and materials science (Pártay et al. 2009). Within this work we also use nested sampling for parameter estimation and model selection.

Multiple nested sampling libraries exist. For gravitational astrophysics it is common to use the dynesty sampler CITE, via the Bilby gravitational wave inference library and we continue to follow this precedent. **TK: we may end up not even using Bilby/dynesty so leaving this section unfilled for now. Do we need a very short description of how nested sampling works?**

3.4 Practical considerations

heterodyneing

pulsar terms For now we will consider the measurement noise to be known, although in principle this too could be estimated.

4 TESTS WITH SYNTHETIC DATA

We go on to discuss our choice of pulsars to make up our PTA in Section 4.1, before deploying these techniques in Sections 4.2, 4.3 for parameter estimation and model selection.

4.1 PTA pulsars

With our Kalman filter and nested sampling techniques in hand, in order to proceed it is necessary to specify a PTA configuration. As discussed, multiple separate PTA detectors exist under the umbrella of the IPTA. Going forward we will take the 47 pulsars that make up the NANOGrav PTA (Arzoumanian et al. 2020). NANOGrav is selected simply as a well-representative example of the typical pulsars that make up a PTA. Our results and formulation are not contingent on the choice of PTA, and naturally extend to other PTAs or PTAs with more pulsars.

Within our state-space formulation, the pulsar evolution is governed by a set of 5 parameters, $\bar{\theta}_{\text{PSR}}$ for each pulsar. The parameters $f_{\text{EM}}(0)$, $\dot{f}_{\text{EM}}(0)$ and d are well specified via existing pulsar datasets.

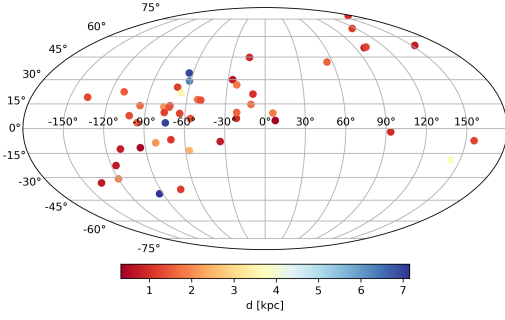


Figure 2. Spatial distribution and distances of NANOGrav pulsars

Parameter	Value
ω	5×10^{-7}
α	1.0
δ	1.0
ψ	2.50
ι	1.0
Φ_0	0.20
h	$1e-2$
σ_p	10^{-13}
σ_m	10^{-10}
T_{obs}	10 years
Δt	7 days

Table 1. GW parameters used for generating synthetic data. There is nothing special about these parameters - they are just chosen arbitrarily.

We take the frequency and frequency derivative as returned from the pulsar datasets to simply be the values now at $t = 0$. The pulsar distances are also known, though less well constrained. Going forward we take the distances returned from the datasets as the true values of the pulsars that make up our synthetic PTA. The specification of γ and σ are more involved. γ specifies an effective timescale of rever- sion to the mean **TK: Need some discussion and though on how to choose these two parameters to be astrophysically reasonable c.f. A. Vargas**

4.2 Parameter estimation

We are now in a position to try to infer the parameters of a GW system. We take our NANOGrav PTA and create a synthetic noisy dataset using the parameters described in Table 1. Given this synthetic data, we can try to use our KF + NS approach to recover some of the parameters. The results for inference on 5 parameters, $\omega, \Phi_0, \psi, \iota, h$ are shown in Fig 3. **TK: likelihood plots for each parameter could also be of interest to include here? Need to expand this section greatly for more astrophysical systems and more unknown parameters**

4.3 Detection

In addition to estimating the parameters of the system, we are also interested in how detectable a GW is using PTA + state space method. We can use our state-space tools to try to solve the problem of GW detection with a PTA i.e. *"Is there evidence of a GW in my data?"* We can frame this as a model selection procedure where we have two models/hypotheses:

- Null Model, M_0 . There is no GW in the data. In this case the

measurement model of the Kalman filter simply returns the frequency states i.e. $g(t, \theta) = 0$

- Alternative model, M_1 . There is a GW in the data. The mea- surement model uses the full expression for $g(t, \theta)$

In order to accept the alternative hypothesis M_1 over M_0 there are two approaches we could take:

(i) The first is a fully Bayesian search over all the parameters for each model, calculating the evidence for each model and then determining the Bayes ratio. This is perhaps the most consistent way, but it is obviously expensive and at this stage we are keen to explore how detectability varies with e.g. GW strain.

(ii) The second method is to recognize that M_0 and M_1 are hi- erarchically nested models and we can perform a likelihood ratio test. That is, given the maximum likelihood estimators $\hat{\theta}$ of the true parameters θ , the likelihood of each model can be calculate. These likelihoods are just point estimates of the Bayes factor numerator/denominators. They can then be compared via the likelihood ratio Λ .

Given the cheap cost we proceed with the second method. For the likelihood ratio test we do not perform any kind of maximum likelihood search over the parameters for each of the models. Instead we just artificially set the maximum likelihood estimators to be equal to the true parameters of the system i.e. $\hat{\theta} = \theta$. We assume that any maximum likelihood algorithm would converge to these parameters. This is obviously an oversimplification but will serve our purposes for now.

Interpreting the likelihood ratio Λ also needs some consideration, since we have to account for the increased model complexity of M_1 . Bayes factors penalise complexity by construction since one must integrate over a larger parameter space. There are many different ways to do this - for now we will consider two: Akaike information criterion (AIC) and Wilks Theorem. For the latter, Wilks' Theorem which states that for a large number of samples ¹ the distribution of the test statistic approaches the chi-squared distribution under the null hypothesis i.e.

$$2 \log \Lambda \rightarrow \chi^2 \quad (55)$$

One can then compute p -values where the number of degrees of freedom is equal to the difference in the number of parameters of the two models; M_1 has 7 extra parameters over M_0 corresponding to the 7 parameters of θ_{GW} . With 7 degrees of freedom and a target tolerance of 5(1) % the test statistic is $\sim 14(18.5)$.

An alternative approach is to use the AIC which is given by,

$$AIC = 2k - 2 \log \mathcal{L} \quad (56)$$

where k is the number of degrees of freedom. The AIC can be computed for each model and the model with the minimum AIC is preferred. This can be straightforwardly mapped into a relative condition

$$\log \mathcal{L}_1 - \log \mathcal{L}_0 > 7 \quad (57)$$

Note this is the same as the Wilks case!

¹ What counts as large? See <https://www.osti.gov/servlets/purl/1529145>

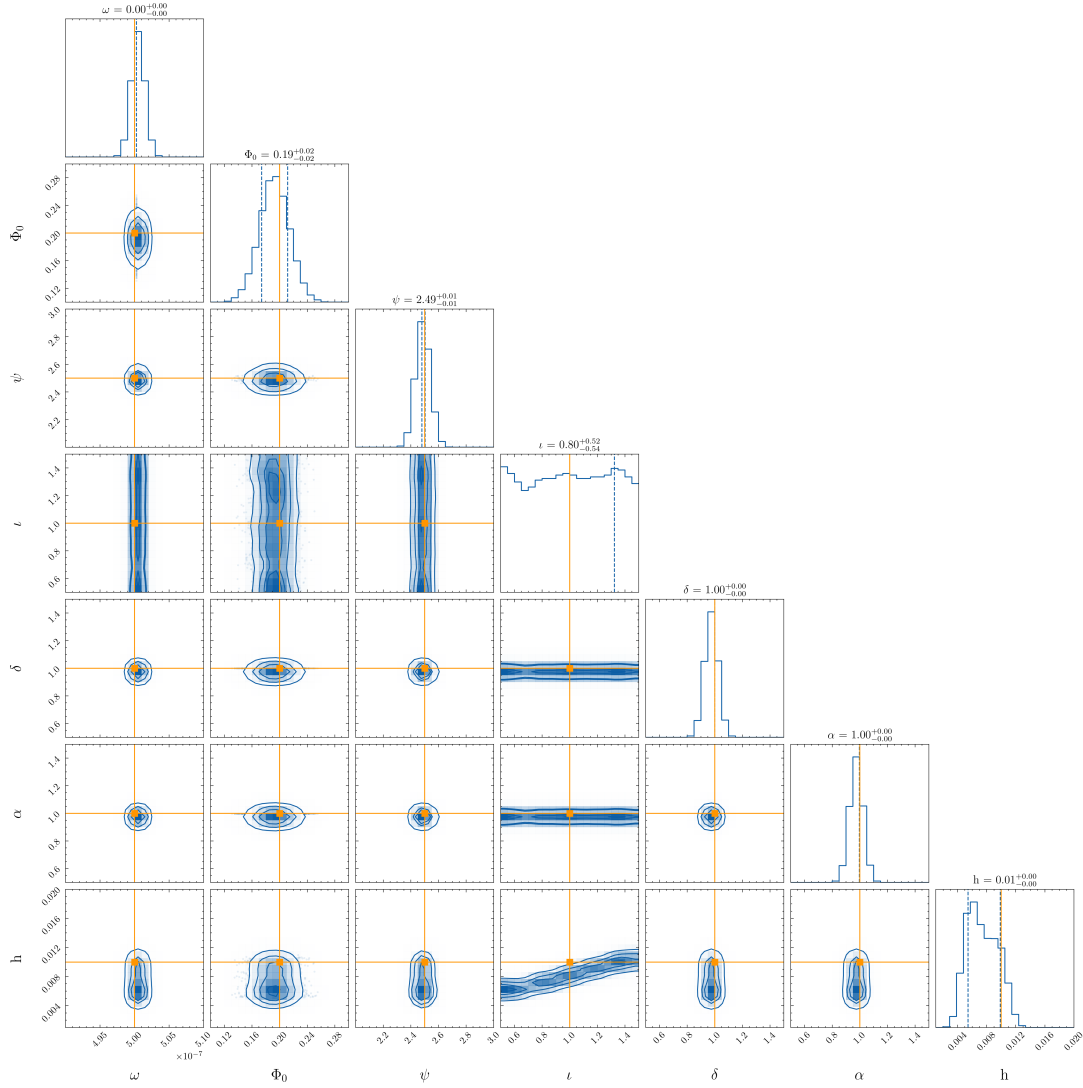


Figure 3. Example corner plot. Aside: for this run the σ_P value fed to the filter is different from that used to generate the data.

5 DISCUSSION

Points to discuss:

- Non constant time sampling? Different pulsars sampled at different times...

6 CONCLUSION

Questions

- PTAs like MSPs for small timing noise. Can we get away with large timing noise, and use more pulsars? Some pulsars are more useful than others, e.g. arXiv 2211.03201
- Can we also estimate radiometer noise? Is this useful?

6.1 References

REFERENCES

Abbott B. P., et al., 2019, *Physical Review X*, 9, 031040
 Abbott R., et al., 2021, *Physical Review X*, 11, 021053

Acernese F., et al., 2015, *Classical and Quantum Gravity*, 32, 024001
 Amaro-Seoane P., et al., 2017, arXiv e-prints, p. arXiv:1702.00786
 Antonelli M., Basu A., Haskell B., 2023, *MNRAS*, 520, 2813
 Antoniadis J., et al., 2022, *MNRAS*, 510, 4873
 Armano M., et al., 2019, arXiv e-prints, p. arXiv:1903.08924
 Arzoumanian Z., et al., 2020, *ApJ*, 905, L34
 Ashton G., et al., 2022, *Nature Reviews Methods Primers*, 2, 39
 Babak S., et al., 2016, *MNRAS*, 455, 1665
 Buchner J., 2021, *The Journal of Open Source Software*, 6, 3001
 Caballero R. N., et al., 2016, *MNRAS*, 457, 4421
 Cordes J. M., Shannon R. M., 2010, arXiv e-prints, p. arXiv:1010.3785
 Ferdman R. D., et al., 2010, *Classical and Quantum Gravity*, 27, 084014
 Feroz F., Hobson M. P., 2008, *MNRAS*, 384, 449
 Gardiner C., 2009, *Stochastic Methods: A Handbook for the Natural and Social Sciences. Springer Series in Synergetics*, Springer Berlin Heidelberg, <https://books.google.com.au/books?id=otg3PQAACAAJ>
 Handley W. J., Hobson M. P., Lasenby A. N., 2015, *MNRAS*, 450, L61
 Hellings R. W., Downs G. S., 1983, *ApJ*, 265, L39
 Hobbs G., Dai S., 2017, *National Science Review*, 4, 707
 Hobbs G., Lyne A. G., Kramer M., 2010, *MNRAS*, 402, 1027
 Kalman R. E., 1960, *Journal of Basic Engineering*, 82, 35
 Kerr M., et al., 2020, *Publ. Astron. Soc. Australia*, 37, e020
 LIGO Scientific Collaboration et al., 2015, *Classical and Quantum Gravity*,

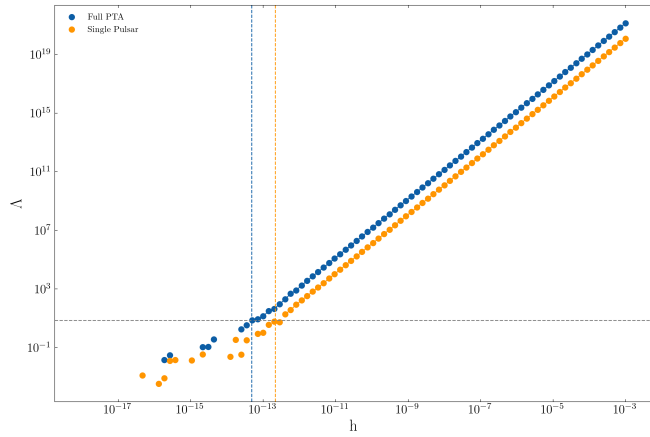


Figure 4. Likelihood ratio vs strain for (a) full PTA and (b) a single randomly chosen pulsar. Horizontal dashed line shows the minimum detectable cutoff, vertical dashed lines are the corresponding GW strains.

32, 074001

- Lam M. T., et al., 2019, *ApJ*, 872, 193
- Lasky P. D., Melatos A., Ravi V., Hobbs G., 2015, *MNRAS*, 449, 3293
- Melatos A., Link B., 2014, *MNRAS*, 437, 21
- Melatos A., Peralta C., Wyithe J. S. B., 2008, *ApJ*, 672, 1103
- Melatos A., O’Neill N. J., Meyers P. M., O’Leary J., 2021, *MNRAS*, 506, 3349
- Meyers P. M., O’Neill N. J., Melatos A., Evans R. J., 2021, *MNRAS*, 506, 3349
- Mukherjee P., Parkinson D., Liddle A. R., 2006, *ApJ*, 638, L51
- Pártay L. B., Bartók A. P., Csányi G., 2009, *arXiv e-prints*, p. arXiv:0906.3544
- Parthasarathy A., et al., 2021, *MNRAS*, 502, 407
- Perera B. B. P., et al., 2019, *MNRAS*, 490, 4666
- Sanidas S. A., Battye R. A., Stappers B. W., 2012, *Phys. Rev. D*, 85, 122003
- Sesana A., Vecchio A., Colacino C. N., 2008, *Monthly Notices of the Royal Astronomical Society*, 390, 192
- Shannon R. M., Cordes J. M., 2010, *ApJ*, 725, 1607
- Simon D., 2006, *Optimal State Estimation: Kalman, H Infinity, and Nonlinear Approaches*. Wiley-Interscience, USA
- Skilling J., 2006, *Bayesian Analysis*, 1, 833
- Tarafdar P., et al., 2022, *Publications of the Astronomical Society of Australia*, 39, e053
- Trassinelli M., 2019, *Proceedings*, 33
- Vargas A., Melatos A., 2023, TBD, 1, 1
- Verbiest J. P. W., Osłowski S., Burke-Spolaor S., 2021, in , *Handbook of Gravitational Wave Astronomy*. p. 4, doi:10.1007/978-981-15-4702-7_4-1
- Wan E., Van Der Merwe R., 2000, in *Proceedings of the IEEE 2000 Adaptive Systems for Signal Processing, Communications, and Control Symposium (Cat. No.00EX373)*. pp 153–158, doi:10.1109/ASSPCC.2000.882463
- Wang Y., 2015, in *Journal of Physics Conference Series*. p. 012019 (arXiv:1505.00402), doi:10.1088/1742-6596/610/1/012019
- Xue X., et al., 2021, *Phys. Rev. Lett.*, 127, 251303
- Zarchan P., Musoff H., 2000, *Fundamentals of Kalman Filtering: A Practical Approach*. Progress in astronautics and aeronautics, American Institute of Aeronautics and Astronautics, https://books.google.com.au/books?id=AQxRAAAAMAJ
- Zhu X.-J., et al., 2015, *Monthly Notices of the Royal Astronomical Society*, 449, 1650

This paper has been typeset from a \LaTeX file prepared by the author.

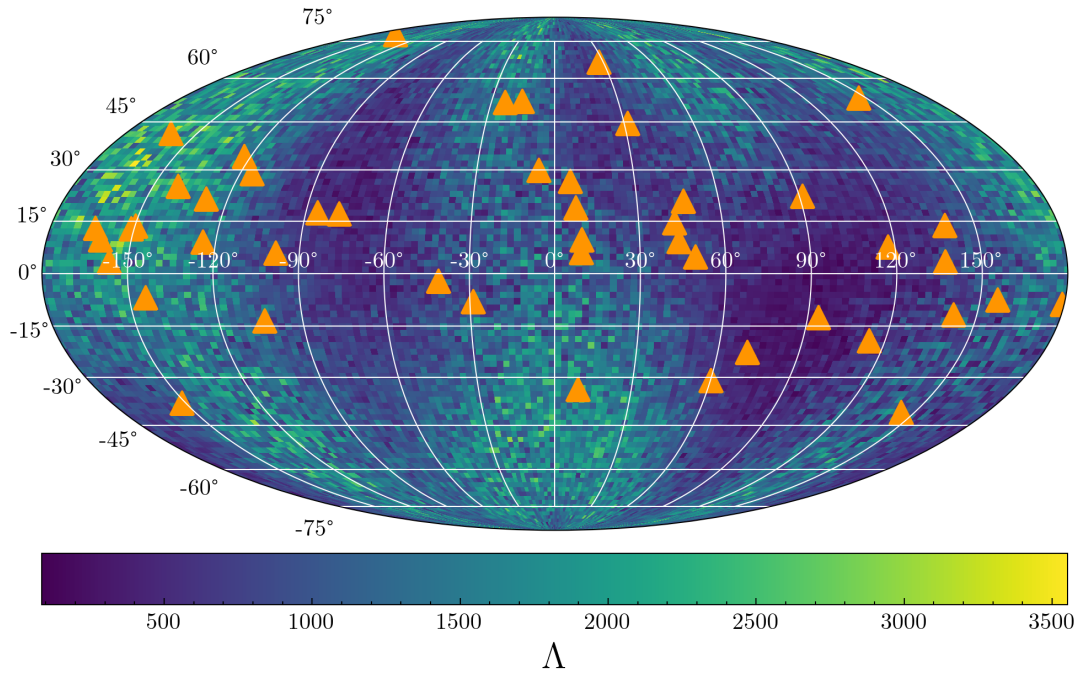


Figure 5. TK: Just a placeholder. Likelihood ratio for a given h . Maybe more interesting, but more expensive, to get minimum detectable h ?